Matter and Radiation at Extremes | RESEARCH ARTICLE | pubs.aip.org/aip/mre

Triggering dynamics of acetylene topochemical polymerization

Cite as: Matter Radiat. Extremes 8, 058402 (2023); doi: 10.1063/5.0151609
Submitted: 23 March 2023 • Accepted: 2 July 2023 •
Published Online: 4 August 2023

Xingyu Tang,[1] Xiao Dong,[2,a)] Chunfang Zhang,[3] Kuo Li,[1,a)] Haiyan Zheng,[1] and Ho-kwang Mao[1]

AFFILIATIONS

[1] Center for High Pressure Science and Technology Advanced Research, Beijing 100193, People's Republic of China
[2] Key Laboratory of Weak-Light Nonlinear Photonics, School of Physics, Nankai University, Tianjin 300071, People's Republic of China
[3] College of Chemistry and Materials Science, Hebei University, Baoding 071002, People's Republic of China

Note: Paper published as part of the Special Topic on High Pressure Science 2023.
[a)] **Authors to whom correspondence should be addressed:** likuo@hpstar.ac.cn and xiao.dong@nankai.edu.cn

ABSTRACT

Topochemical reactions are a promising method to obtain crystalline polymeric materials with distance-determined regio- or stereoselectivity. It has been concluded on an empirical basis that the closest intermolecular C···C distance in crystals of alkynes, $d_{(C\cdots C)min}$, should reach a threshold of ~3 Å for bonding to occur at room temperature. To understand this empirical threshold, we study here the polymerization of acetylene in the crystalline state under high pressure by calculating the structural geometry, vibrational modes, and reaction profile. We find $d_{(C\cdots C)min}$ to be the sum of an intrinsic threshold of 2.3 Å and a thermal displacement of 0.8 Å (at room temperature). Molecules at the empirical threshold move via several phonon modes to reach the intrinsic threshold, at which the intermolecular electronic interaction is sharply enhanced and bonding commences. A distance–vibration-based reaction picture is thus demonstrated, which provides a basis for the prediction and design of topochemical reactions, as well as an enhanced understanding of the bonding process in solids.

I. INTRODUCTION

Topochemical reactions are a kind of solid-state reaction that depend strongly on the stacking of the reactant molecules.[1,2] Initiated by heating, irradiation or compression, such reactions can be used to produce a variety of interesting molecules and polymeric materials with desirable optoelectronic and mechanical properties.[3–5] They are also highly atom-economic, with excellent regio- and stereo-selectivity, and they sometimes result in single-crystal-to-single-crystal transformation.[6,7] Since the first systematic exploration of the [2 + 2] reaction of substituted cinnamic acids by Schmidt in 1964,[2,8] more and more topochemical reactions have been developed, including [4 + 4], [4 + 2], and [3 + 2] cycloaddition reactions, as well as 1,4- or 1,6-addition reactions of diynes, dienes, trienes, and triynes.[1,7,9–12] All these investigations suggest that suitable stacking of the molecules and short spacing between the reactive groups are key to topochemical reactions, and some topochemical postulates have been proposed to provide guidance for the design of the reactions.[2] For instance, the distance between C=C double bonds in [2 + 2] cycloaddition reactions should be in the range of 3.5–4.2 Å, while the ideal distance for the topochemical polymerization of diacetylene is $d_{(C1\cdots C4')} < 4$ Å, with stacking spacing ≈5 Å.[7,8] However, most of the proposed distances have been determined from the original and ground-state crystal structures, rather than the structure at the moment of the photo- or thermal reactions, and therefore they are not closely related to the intrinsic reaction criteria, nor are they really predictive.[13,14]

Recently, pressure-induced polymerization (PIP) has attracted widespread attention, given that the application of pressure can continuously adjust the intermolecular distance and drive molecules to spontaneously react, where a critical structure before the reaction is clearly defined.[15] A uniform empirical shortest intermolecular C···C distance at threshold, $d_{(C\cdots C)min}$, can be derived from PIP reactions at room temperature (RT), suggesting that it is directly related to the nature of the functional groups involved.[16] As summarized in Table I, although the reaction pressure varies, alkynes always react when $d_{(C\cdots C)min}$ reaches ~3 Å. For example, acetylene dicarboxylic acid polymerizes to form crystalline percarboxylpolyacetylene at $d_{(C\cdots C)min} \approx 3.1$ Å, which is almost the same value as for acetylene.[5,17] By contrast, aromatics react at ~2.8 Å owing to

TABLE I. Intermolecular threshold distances for PIP at RT without correction of thermal fluctuation given by experiments.

Molecular crystal	$d_{(C\cdots C)min}$ (Å)	Pressure (GPa)	Functional group
Acetylene (C_2H_2)[17]	3.1	5.7	Alkynyl
Acetylene dicarboxylic acid (HOOC–C≡C–COOH)[5]	3.1	8	
Monosodium acetylide ($NaHC_2$)[18]	2.9	11	
1-propargyl-4-amino-3, 5- dinitropyrazole[19]	3.3	11.3	
Benzene (C_6H_6)[20]	2.8	18	Phenyl
Benzene–hexafluorobenzene (C_6H_6–C_6F_6)[21]	2.8	20	
1,4-diphenylbutadiyne (DPB)[22]	3.2	10	Alkynyl-phenyl
1,3,5-triethynylbenzene (TEB)[23]	3.4	4	

their relative inertness,[20,21] and alkynylarenes have a longer distance owing to their concerted bonding.[22,23]

This empirical threshold $d_{(C\cdots C)min}$ is an excellent parameter to predict topochemical reactions under external pressure. However, its physical and chemical basis is still unknown. A quantitative understanding of this threshold is critical for designing rational syntheses via topochemical reactions under pressure and is even important for solid-state heat/irradiation-initiated reactions. An investigation of the PIP of benzene crystals established a link between the maximum fluctuation of $d_{C\cdots C}$ between rigid molecules on the one hand and the temperature T and the phonon frequency ν (expressed as wavenumber) of the lowest optical translational mode at the Γ-point of the Brillouin zone on the other, with the square of the molecular displacement x being given by

$$x^2 = \frac{k_B T}{M(2\pi c\nu)^2}, \tag{1}$$

where k_B is Boltzmann's constant, M is the molecular mass, and c is the speed of light.[20] By subtracting the thermal fluctuations from the experimentally determined distance between rigid molecules under different pressure–temperature conditions, it was found that the distance converged to ~2.6 Å as a trigger threshold. This work revealed the important role of phonons in PIP, but the underlying physical mechanism remained obscure, and the complex reaction pathways of benzene cannot be fully understood from this model.

Acetylene is the simplest alkyne, and its polymerization is a textbook addition reaction that initiated the study of conductive polymers, making it a perfect model to study the origin of the threshold distance and the reaction selectivity.[24] It was reported that acetylene polymerized to *trans*-polyacetylene at 4 GPa and RT,[25] or to *cis*-polyacetylene at 12 GPa and 77 K.[26] In the most recent crystallographic investigation, acetylene was found to polymerize at 5.7 GPa and RT via a topochemical route, forming *cis*-polyacetylene and subsequently nano-graphane.[17] *In situ* neutron diffraction and molecular dynamics (MD) simulations disclosed that the bonding started at $d_{(C\cdots C)min}$ = 3.1 Å. In the present paper, we adopt a computational approach to probe the threshold distance of acetylene, decompose the reaction process of PIP, reveal the underlying physics, and uncover the origin of the RT experimental threshold distance of 3.1 Å. These quantitative results should also help in understanding other topochemical addition bonding process.

II. PIP OF ACETYLENE AT 0 K

To investigate the structural variations under applied pressure, we first optimized the crystal structure of acetylene at 0 K and external pressure. Starting with the experimental critical structure at RT and 5.7 GPa reported in Ref. 17, stress-equilibrated structures were obtained under different pressures. In our calculation, the optimized structure at 0 GPa had the closest lattice parameters and $d_{(C\cdots C)min}$ to the experimental critical structure (experimental 5.7 GPa; for a comparison, see Table S1 in the supplementary material), and so we used the optimized result at 0 GPa to represent the experimental crystal structure at 5.7 GPa. We investigated the pressure range from 0 to 30 GPa and found that acetylene polymerized above 28.8 GPa. Representative structures and geometric parameters are displayed in Fig. 1. The acetylene molecules lie on the b–c plane. With increasing pressure, the cell parameters shrink with a decreasing rate until the acetylene is about to polymerize. a is the most compressed, followed by c, and b is the least. For the two closest intermolecular distances, d1 in the a–c plane (potentially leading to the *cis*-polymer) decreases faster than d2 before reaction. In addition, the angle ∠C–C–c (∠1) continues to increase, while ∠H–H–c (∠2) does not do so before the reaction occurs, which results in bending of the H–C≡C–H molecule [smaller bond angle ∠3, marked in Fig. 1(a)]. The equilibrated C≡C bond lengthens by about 1% just before reaction, indicating a weakening.

At 28.9 GPa, acetylene polymerized during optimization. We then concluded that the $d_{(C\cdots C)min}$ (d1 = 2.3 Å) at 0 K and 28.8 GPa was the intrinsic threshold distance of this PIP. We performed an MD simulation at 28.8 GPa and a limited temperature (50 K) to visualize the bonding process, in which the chain polymer was first generated along the $a + c/a - c$ direction (Fig. S1, supplementary material), consistent with Ref. 17. For the crystal structures obtained during optimization and MD simulation, we studied the relationship between intermolecular electronic interaction and $d_{C\cdots C}$ by single-point calculations. The Mayer bond order of the intermolecular C···C bond and the value of the electron localization function (ELF) at the midpoint of the bond, which respectively represent the sharing of electron pairs and the electronic localization between these two carbon atoms, are plotted vs bond length in Fig. 2. Both curves have turning points near 2.3 Å, suggesting enhanced intermolecular electron interaction at that distance. This weakens the repulsion between adjacent molecules and corresponds to the tipping point of bonding. Thus, we can conclude that intermolecular bonding in the acetylene crystal commences when the 2.3 Å intrinsic threshold distance is reached.

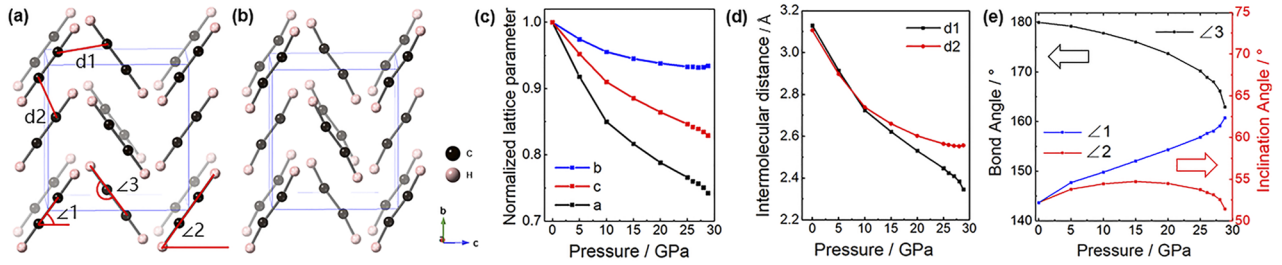

FIG. 1. Optimized crystal structure of C_2H_2 at (a) 0 GPa and (b) 25 GPa. (c) Relative changes in unit cell parameters. (d) Selected $d_{C\cdots C}$ and (e) angles in the crystal as functions of pressure. d1 is $d_{C\cdots C}$ on the *a*–*c* plane, and d2 is $d_{C\cdots C}$ almost on the *a*–*b* plane. ∠1 or ∠2 is the angle between the *c* axis and the line between two carbon/hydrogen atoms, and ∠3 is the H–C–C bond angle.

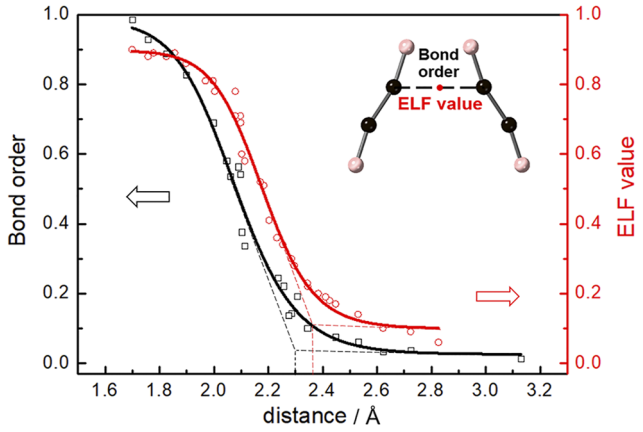

FIG. 2. Electronic properties of the intermolecular C· · ·C bond vs bond length. The bonding proceeds in three stages. At about 2.3 Å, the Mayer bond order (black) and the ELF value at the midpoint of the bond (red) sharply increase, suggesting the onset of bonding.

III. VIBRATIONAL ANALYSIS

To probe the dynamic properties of the acetylene crystal and find the possible reactions involved, we first calculated the phonon spectrum of the structure at 0 K and threshold pressure for reference. On forcing the last stress-equilibrated optimized structure before reaction (28.8 GPa) to a little higher pressure (29 GPa) with limited optimization steps, an imaginary frequency appeared at the Γ-point and T-point (0.5, 0, −0.5), as shown in Fig. 3(a). The imaginary mode at the Γ-point (−76 cm^{-1}) belongs to an optical branch originating from the lattice vibrational mode (Fig. S2, supplementary material), which is −44 cm^{-1} at the T-point. Another three vibrational modes with imaginary frequencies are also found at −44 cm^{-1} at the T-point, corresponding to the acoustic branches. This tells us that both the vibrations with the T-point symmetry and those with the Γ-point symmetry (symmetry of vibrations, or collective behaviors of molecular motion) should be highly focused.

In RT experiments, the static external pressure changes the equilibrated configuration, while it is always the thermal displacement of atoms leading to a decrease in $d_{C\cdots C}$ that initiates the bonding. Therefore, we calculated the phonon spectrum of the structure at 0 GPa [experimental 5.7 GPa, Fig. 3(c)] and analyzed the vibrational modes in detail to help demonstrate the effect of temperature. Figure S3 (supplementary material) presents details of 48 normal vibrational modes at the Γ-point, which are closely related to molecular motions. Modes with wavenumber below 300 cm^{-1} are lattice vibrational modes (modes 1–20 in Fig. S3). Modes with wavenumbers in the range 600–900 cm^{-1} (modes 21–36) are bending modes. Stretching modes for C–C bonds (modes 37–40) and C–H bonds (modes 41–48) are located around 2000 and 3100 cm^{-1},

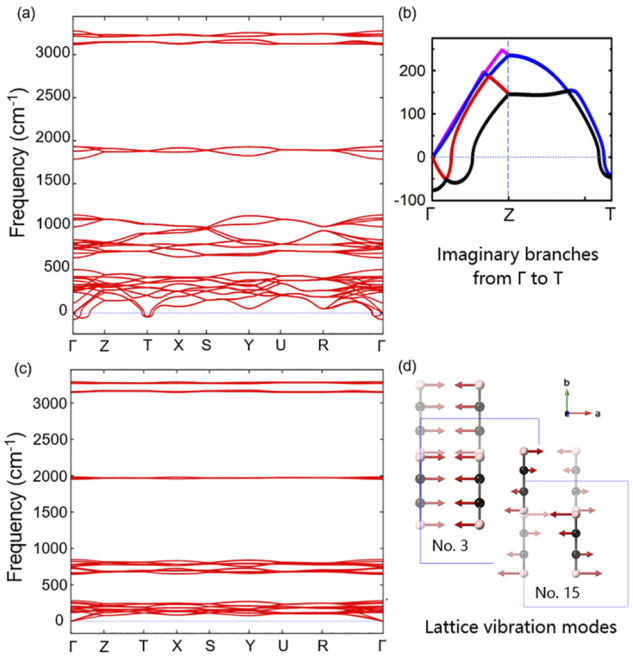

FIG. 3. Phonon spectra of the acetylene crystal and some of the vibrational modes at the Γ-point. (a) Spectrum of the optimized structure at 29 GPa. (b) Four phonon branches with imaginary frequencies from the Γ-point to the T-point (0.5, 0, −0.5) at 29 GPa. (c) Spectrum at 0 GPa (experimental 5.7 GPa). In the high-frequency part, the phonon dispersion curves are nearly horizontal. (d) Illustrations of two typical lattice vibrations leading to a decrease in $d_{C\cdots C}$, originating from molecular translations and rotations.

respectively. Among these vibrations, lattice vibrational modes, corresponding to translations or rotations of the four molecules, are the major contributors to the fluctuations in $d_{C\cdots C}$. According to the analysis in Sec. II, we focus on the decrease of d1. Let us take the translations along a as an example (modes 1–4 in Fig. S3). In modes 1 (acoustic branch) and 2, the adjacent carbon atoms from neighboring molecules move in the same direction with $d_{C\cdots C}$ unchanged, whereas in modes 3 and 4, they move in opposite directions to each other and compress $d_{C\cdots C}$. As a result, about half of the lattice vibrational modes, specifically modes 3, 4, 11, 12, 15, 16, 19, and 20 (group 1) at the Γ-point, play the major roles in decreasing the value of $d_{C\cdots C}$. By contrast, modes 1, 2, 9, 10, 13, 14, 17, and 18 (group 2) have little effect. For the vibrational modes with T-point symmetry, it is still the lattice vibrational modes that cause $d_{C\cdots C}$ to decrease, which will be illustrated later. Thus, the vibrations closely related to intermolecular bonding have been determined.

IV. THERMAL VIBRATIONS AND INDUCED REACTION

In solids, the collective behaviors of atoms correspond to phonon modes. For a system of N atoms in the solid state, there are $3N$ vibrational degrees of freedom, corresponding to $3N$ phonon branches. For simplicity, a classical physical model is used here when dealing with the total thermal energy of the system, i.e., this is given by $3Nk_BT$ at a relatively high temperature T according to the Dulong–Petit law.

When we focus on a certain Q-point in the Brillouin zone (or a certain wave vector) from the viewpoint of classical physics, the $3N$ corresponding vibrational modes at this point, with frequencies given by the phonon dispersion relations, are mutually independent. In this situation, the average thermal energy of each mode is the same, giving k_BT in total. Thus, under the harmonic approximation, the maximum displacement of N atoms in the jth phonon mode at this Q-point can be represented as

$$\sum_{i}^{N\ \text{atoms}} \frac{1}{2} m_i \| \overrightarrow{x_{\mathrm{i,j,max}}} \|^2 = \frac{k_B T}{(2\pi c \nu_j)^2}, \tag{2}$$

where $\overrightarrow{x_{\mathrm{i,j,max}}}$ is the maximum displacement of the ith atom determined by the jth phonon mode, ν_j represents the frequency of this mode (expressed as wavenumber), and m_i is the mass of the ith atom. Equation (2) is an enhancement of Eq. (1) and provides a general illustration of how phonon modes contribute to atomic motion in solids. It also demonstrates that low-frequency vibrations, lattice modes for example, contribute more to the decrease in $d_{C\cdots C}$ than high-frequency vibrations such as stretching modes. With Eq. (2), we can estimate the instantaneous shortest $d_{C\cdots C}$ in the acetylene system at RT.

In the limiting case, the maximum displacement of a carbon atom is

$$\overrightarrow{x_{\mathrm{C,max}}} = \sum_{j} \overrightarrow{x_{\mathrm{C,j,max}}}. \tag{3}$$

The instantaneous shortest $d_{C\cdots C}$ is obtained when all the modes contributing to the reduction in d1 are applied together. On the basis of the above analysis, both lattice vibrational modes satisfying Γ-point symmetry and those satisfying T-point symmetry can induce a significant decrease in $d_{C\cdots C}$. At the Γ-point, it is the vibrational modes in group 1 that are active in this respect. However, for the vibrational modes at the T-point, there are extra phase differences in the molecular vibrations compared with the modes at the Γ-point (Fig. S4, supplementary material). Both vibrational modes in group 1 and those in group 2 at the T-point can induce a decrease in $d_{C\cdots C}$, but these reductions occur in different diagonal directions ($a + c/a - c$) respectively. Owing to their lower frequencies, the modes in group 2 lead to larger

TABLE II. Phonon frequencies of the lattice vibrational modes at the T-point and the maximum displacements of carbon atoms in the optimized structure at 0 GPa (experimental 5.7 GPa). Displacements are displayed as projections on the coordinate axes.

			Displacement of a carbon atom (Å)		
Vibrational mode	No.	Frequency (cm^{-1})	Δx	Δy	Δz
Translational	1	113	0.103	0	0
	2	146	0.080	0	0
	9	113	0	0	0.103
	10	189	0	0	0.062
	Total = $\sum \Delta x, \Delta y$ or Δz		0.183	0	0.165
Librational	13	165	0.064	0	0
	14	146	0.073	0	0
	17	238	0	0.027	0.035
	18	146	0	0.045	0.058
	Total = $\sum \Delta x, \Delta y$ or Δz		0.137	0.072	0.093
Total displacement in a–c plane			0.411		

atomic displacements of carbon atoms at the T-point; see Fig. S5 (supplementary material), which shows in greater detail part of the lattice vibrational modes from the Γ-point to the T-point in Fig. 3(c).

The maximum atomic displacements of carbon atoms induced by the modes in group 2 at the T-point were calculated according to Eq. (2) and are listed in Table II. According to Eq. (3), each of the two carbon atoms can move ~0.4 Å to its limiting position via thermal vibrations, with the translational vibrations contributing about two-thirds of this movement and the librational vibrations about one-third. Interestingly, the movement is precisely along the C···C direction, as shown in Fig. 4, and so the maximum fluctuation of $d_{C\cdots C}$ is the sum of two opposite displacements, which is ~0.8 Å. Thus, $d_{C\cdots C}$ decreased from 3.1 to 2.3 Å, the same as the aforementioned intrinsic threshold distance at 0 K. Parallel investigation of the Γ-point situation (Table S2, supplementary material, which should be compared with Table II) shows that the maximum displacement is ~0.3 Å for one carbon atom, which is smaller than that at the T-point and is therefore less important to the PIP.

The positions of the hydrogen atoms in Fig. 4 were determined by an additional optimization with the carbon atoms frozen since these were also affected by other vibrational modes such as bending modes. We thereby obtained a transient "threshold model" structure by adding eight vibrational displacements to the experimentally determined crystal structure at RT and 5.7 GPa. In the model, the minimum instantaneous $d_{C\cdots C}$ reproduced the local structure of the intrinsic threshold model well at 0 K and 28.8 GPa. Thus, we could conclude that the experimentally observed threshold distance 3.1 Å is actually the sum of an intrinsic threshold of 2.3 Å and a vibrational contribution of 0.8 Å.

Finally, we performed variable cell nudged elastic band (vc-NEB) calculations to investigate the relationship between the transient "threshold model" and the transition state of PIP from the perspective of enthalpy. First, the minimum energy path (MEP) from acetylene crystal to *cis*-polyacetylene was searched in a $2a \times 1b \times 2c$ supercell. The energy curve is displayed in Fig. 5. In the state with the highest enthalpy (like a transition state, "TS"), the instantaneous shortest intermolecular C···C distance is about 1.6 Å

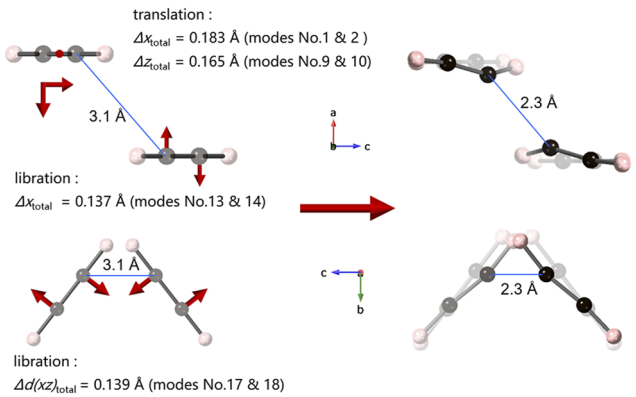

FIG. 4. Vibrational displacement of carbon atoms from the equilibrated position with T-point symmetry applied. The instantaneous $d_{C\cdots C}$ at RT becomes 2.3 Å and reaches the threshold for intermolecular bonding.

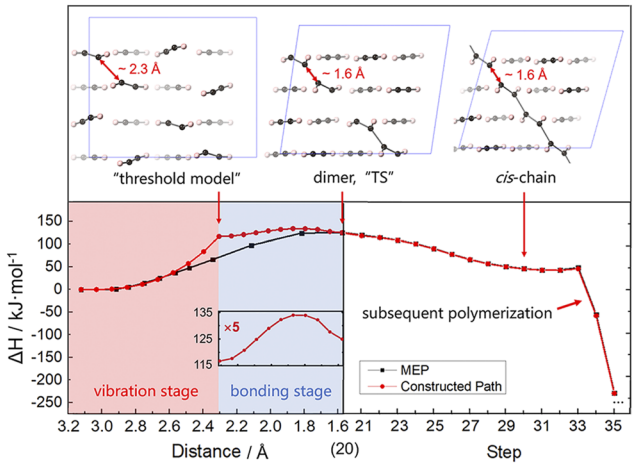

FIG. 5. Reaction curve from acetylene to polyacetylene in the crystal. The MEP is shown as the black line, and the pathway through the transient "threshold model" is shown as the red line. The left part of each curve describes the enthalpy change of the supercell as the instantaneous $d_{C\cdots C}$ varies until intermolecular bonding occurs. The right part is the subsequent reaction displayed in steps. The bonding stage on the new path is rescaled for clarity. Three representative structures along the constructed path are illustrated. The enthalpies of the "threshold model" and the "TS" are almost the same.

within a dimer. The activation energy is around 2.7 eV per supercell, which is ~134 kJ/(mol C–C bond). As polymerization proceeds, *cis*-polyacetylene chains are formed, accelerating the reaction of other molecules. Finally, *cis*-polyacetylene is formed. Based on the MEP, we constructed the pathway via the transient "threshold model," also shown in Fig. 5 (red line). On this pathway, other structures between the initial state and the "TS" were regenerated by linear interpolation of the lattice parameters and the atomic positions. In the MEP, the unit cell changes first, and only once the intermolecular spacing has become short enough does the reaction begin (Fig. S6, supplementary material). On the new pathway, however, when 2.3 Å is reached via vibrations, intermolecular bonding is facilitated, leading to an almost flat energy curve in the bonding stage. This process is similar to the spontaneous reaction at 0 K and 28.8 GPa and demonstrates that vibrations can provide enough energy for the molecules to overcome the "TS" if they move to the vibrational maximum at RT.

An electronic interaction analysis of the transient "threshold model" also supports the similarity of the two reaction processes. The intermolecular bond order is 0.15, and the ELF value at the midpoint is 0.25, which is in accord with tipping point at 28.8 GPa in Fig. 2, implying a similar electronic interaction. Thus, we can conclude that owing to thermal vibrations, the $d_{(C\cdots C)min}$ under experimental conditions (3.1 Å) is dynamically compressed to the intrinsic threshold distance for PIP (2.3 Å), inducing the bonding of acetylene molecules as a trigger of the reaction. Additionally, all the structures in the two reaction processes were spin-unpolarized (the transient "threshold model" for example; see Fig. S7, supplementary material). In other words, no single electron appeared in the reaction processes. The same conclusion was reported in the benzene system in Ref. 20.

MD simulations also were carried out to provide an intuitive proof. The result of Pair distribution function (PDF) evolution are displayed in Fig. S8 (supplementary material), where a threshold for acetylene at about 2.3 Å can be observed, in excellent agreement with the conclusion above.

With the above understanding, we can now predict the influence of temperature quantitatively. Without taking changes in frequencies into consideration, the vibrational displacement is approximately proportional to the square root of temperature. Therefore, the contributions of thermal vibration are 0.9, 1.0, and 0.7 Å for 400, 500, and 200 K, respectively. The experimental threshold distances then become 3.2 Å at 400 K, 3.3 Å at 500 K, and 3.0 Å at 200 K, which are instructive values with regard to the selective synthesis of *cis*- or *trans*-polyacetylene.

V. CONCLUSION

In summary, our study has revealed an intrinsic threshold distance 2.3 Å for acetylene crystals at 0 K, where intermolecular C···C interaction is significantly enhanced. We have found that lattice vibrations are crucial for pressure-induced polymerization, calculated their contributions to the decrease in $d_{C\cdots C}$ at room temperature, and have applied this finding to the experimentally determined threshold structure. We have obtained a transient "threshold model" with an instantaneous $d_{C\cdots C}$ of 2.3 Å, which perfectly reproduces the intrinsic threshold and thus demonstrates how the reaction is initiated by vibrations. This model, which can be described as "intrinsic threshold + vibration maximum," perfectly explains the experimental threshold of 3.1 Å for acetylene, and can also be applied on other alkyne systems. Our work has provided a quantitative understanding of the distance threshold and the effect of temperature in topochemical reactions, and the results obtained here will be useful for developing novel topochemical reactions as well as tailored syntheses of regio- and stereospecific polymeric materials.

SUPPLEMENTARY MATERIAL

Computational details, elaborate illustration of vibrational modes, result of MD simulation and supplementary figures and tables are displayed in supplementary material.

ACKNOWLEDGMENTS

The authors acknowledge the support of the National Natural Science Foundation of China (NSFC) (Grant Nos. 22022101, 21875006, 11704024, and 12174200). The authors also acknowledge support from the National Key Research and Development Program of China (Grant No. 2019YFA0708502) and from the Nature Science Foundation of Tianjin (Grant No. 20JCYBJC01530).

AUTHOR DECLARATIONS

Conflict of Interest

The authors have no conflicts to disclose.

Author Contributions

Xingyu Tang: Formal analysis (lead); Writing – original draft (lead). **Xiao Dong**: Formal analysis (supporting); Funding acquisition (supporting). **Chunfang Zhang**: Formal analysis (supporting). **Kuo Li**: Conceptualization (lead); Formal analysis (supporting); Funding acquisition (lead); Project administration (lead); Writing – review & editing (lead). **Haiyan Zheng**: Funding acquisition (supporting); Writing – review & editing (supporting). **Ho-kwang Mao**: Supervision (lead).

DATA AVAILABILITY

The data that support this study are available from the corresponding authors upon reasonable request.

REFERENCES

[1]K. Hema, A. Ravi, C. Raju, J. R. Pathan, R. Rai, and K. M. Sureshan, "Topochemical polymerizations for the solid-state synthesis of organic polymers," Chem. Soc. Rev. **50**, 4062 (2021).
[2]K. Biradha and R. Santra, "Crystal engineering of topochemical solid state reactions," Chem. Soc. Rev. **42**, 950 (2013).
[3]C. Sauteret, J. P. Hermann, R. Frey, F. Pradère, J. Ducuing, R. H. Baughman, and R. R. Chance, "Optical nonlinearities in one-dimensional-conjugated polymer," Phys. Rev. Lett. **36**, 956 (1976).
[4]T. Kato, M. Yasumatsu, C. Origuchi, K. Tsutsui, Y. Ueda, and C. Adachi, "High carrier mobility of 3.8 cm^2 V^{-1} s^{-1} in polydiacetylene thin films polymerized by electron beam irradiation," Appl. Phys. Express **4**, 091601 (2011).
[5]X. Wang, X. Tang, P. Zhang, Y. Wang, D. Gao, J. Liu, K. Hui, Y. Wang, X. Dong, T. Hattori, A. Sano-Furukawa, K. Ikeda, P. Miao, X. Lin, M. Tang, Z. Zuo, H. Zheng, K. Li, and H.-k. Mao, "Crystalline fully carboxylated polyacetylene obtained under high pressure as a Li-ion battery anode material," J. Phys. Chem.Lett. **12**, 12055 (2021).
[6]L. Dou, Y. Zheng, X. Shen, G. Wu, K. Fields, W. C. Hsu, H. Zhou, Y. Yang, and F. Wudl, "Single-crystal linear polymers through visible light-triggered topochemical quantitative polymerization," Science **343**, 272 (2014).
[7]J. W. Lauher, F. W. Fowler, and N. S. Goroff, "Single-crystal-to-single-crystal topochemical polymerizations by design," Acc. Chem. Res. **41**, 1215 (2008).
[8]G. M. J. Schmidt, "Topochemistry. Part III. The crystal chemistry of some *trans*-cinnamic acids," J. Chem. Soc. **1964**, 2014.
[9]K. Hema and K. M. Sureshan, "Topochemical azide–alkyne cycloaddition reaction," Acc. Chem. Res. **52**, 3149 (2019).
[10]M. J. Kory, M. Wörle, T. Weber, P. Payamyar, S. W. van de Poll, J. Dshemuchadse, N. Trapp, and A. D. Schlüter, "Gram-scale synthesis of two-dimensional polymer crystals and their structure analysis by X-ray diffraction," Nat. Chem. **6**, 779 (2014).
[11]J. Xiao, M. Yang, J. W. Lauher, and F. W. Fowler, "A supramolecular solution to a long-standing problem: The 1,6-polymerization of a triacetylene," Angew. Chem., Int. Ed. **39**, 2132 (2000).
[12]P. Kissel, R. Erni, W. B. Schweizer, M. D. Rossell, B. T. King, T. Bauer, S. Götzinger, A. D. Schlüter, and J. Sakamoto, "A two-dimensional polymer prepared by organic synthesis," Nat. Chem. **4**, 287 (2012).
[13]W. L. Dilling, "Organic photochemistry. XVII. Polymerization of unsaturated compounds by photocycloaddition reactions," Chem. Rev. **83**, 1 (1983).
[14]M. Hasegawa, "Photopolymerization of diolefin crystals," Chem. Rev. **83**, 507 (1983).
[15]C.-S. Yoo, "Chemistry under extreme conditions: Pressure evolution of chemical bonding and structure in dense solids," Matter Radiat. Extremes **5**, 018202 (2020).
[16]F. Li, J. Xu, Y. Wang, H. Zheng, and K. Li, "Pressure-induced polymerization: Addition and condensation reactions," Molecules **26**, 7581 (2021).

[17]J. Sun, X. Dong, Y. Wang, K. Li, H. Zheng, L. Wang, G. D. Cody, C. A. Tulk, J. J. Molaison, X. Lin, Y. Meng, C. Jin, and H.-k. Mao, "Pressure-induced polymerization of acetylene: Structure-directed stereoselectivity and a possible route to graphene," Angew. Chem., Int. Ed. **56**, 6553 (2017).
[18]J. Han, X. Tang, Y. Wang, Y. Wang, Y. Han, X. Lin, X. Dong, H. H. Lee, H. Zheng, K. Li, and H.-k. Mao, "Pressure-induced polymerization of monosodium acetylide: A radical reaction initiated topochemically," J. Phys. Chem. C **123**, 30746 (2019).
[19]G. Qi, S. Song, Z. Deng, D. Huang, F. Chen, B. Yan, H. Gou, Q. Zhang, and Y. Wang, "Pressure-induced topochemical polymerization toward advanced energetic materials," CCS Chem (published online) (2022).
[20]L. Ciabini, M. Santoro, F. A. Gorelli, R. Bini, V. Schettino, and S. Raugei, "Triggering dynamics of the high-pressure benzene amorphization," Nat. Mater. **6**, 39 (2007).
[21]Y. Wang, X. Dong, X. Tang, H. Zheng, K. Li, X. Lin, L. Fang, G. Sun, X. Chen, L. Xie, C. L. Bull, N. P. Funnell, T. Hattori, A. Sano-Furukawa, J. Chen, D. K. Hensley, G. D. Cody, Y. Ren, H. H. Lee, and H.-k. Mao, "Pressure-induced Diels–Alder reactions in C_6H_6-C_6F_6 cocrystal towards graphane structure," Angew. Chem., Int. Ed. **58**, 1468 (2000).
[22]P. Zhang, X. Tang, Y. Wang, X. Wang, D. Gao, Y. Li, H. Zheng, Y. Wang, X. Wang, R. Fu, M. Tang, K. Ikeda, P. Miao, T. Hattori, A. Sano-Furukawa, C. A. Tulk, J. J. Molaison, X. Dong, K. Li, J. Ju, and H.-k. Mao, "Distance-selected topochemical dehydro-Diels–Alder reaction of 1,4-diphenylbutadiyne toward crystalline graphitic nanoribbons," J. Am. Chem. Soc. **142**, 17662 (2020).
[23]Y. Li, X. Tang, P. Zhang, Y. Wang, X. Yang, X. Wang, K. Li, Y. Wang, N. Wu, M. Tang, J. Xiang, X. Lin, H. H. Lee, X. Dong, H. Zheng, and H.-k. Mao, "Scalable high-pressure synthesis of sp^2–sp^3 carbon nanoribbon via [4 + 2] polymerization of 1,3,5-triethynylbenzene," J. Phys. Chem. Lett. **12**, 7140 (2021).
[24]H. Shirakawa, E. J. Louis, A. G. MacDiarmid, C. K. Chiang, and A. J. Heeger, "Synthesis of electrically conducting organic polymers: Halogen derivatives of polyacetylene, $(CH)_x$," J. Chem. Soc. Chem. Commun. **1977**, 578.
[25]M. Sakashita, H. Yamawaki, and K. Aoki, "FT-IR study of the solid state polymerization of acetylene under pressure," J. Phys. Chem. **100**, 9943 (1996).
[26]C. C. Trout and J. V. Badding, "Solid state polymerization of acetylene at high pressure and low temperature," J. Phys. Chem. A **104**, 8142 (2000).